

# Effects of geometry and material on the insertion of very small neural electrode.

Shaun P. Marshall, Wei-Chen Lin, Paras R. Patel, Albert J. Shih, *Member, ASME*, Cynthia A. Chestek, *Member, IEEE*

**Abstract**— For neural probes to be used chronically for years in the human body, they must provoke minimal scarring. Recently, a number of groups have reported substantially reduced scar tissue using cellular scale electrodes below 15  $\mu\text{m}$  in size. This size scale is accessible to manufacturing techniques, but can be very difficult to insert in the brain for most common electrode materials. In this study, we explore the design space available to cellular scale electrodes that will self-insert into the brain. First a mathematical model is developed using beam buckling equations for different materials and geometries. Buckling mode was found to be one fixed and one hinged end resulting in a mode conditional constant of,  $n = 2.045$ . Model predicts insertion success between 90 – 100% for a 6.8  $\mu\text{m}$  diameter electrode and was used to approximate applied force as 750  $\mu\text{N}$  which is close to reference data of 780  $\mu\text{N}$  [1]. Second, we developed a PVC phantom that mimics the brain's elastic modulus. This phantom was matched to insertion success data obtained from carbon fiber arrays [1]. Overall, these results enable studies to be conducted on other proposed cellular scale electrodes prior to animal testing or large scale fabrication.

## I. INTRODUCTION

Brain machine interfaces have the capacity to bridge across pathological gaps in the nervous system caused by injury or disease using implantable devices that sense or stimulate neurons. For clinical viability, these devices need to last a long time. This is difficult since these chronically implanted arrays can cause persistent scarring which can extend out to 250  $\mu\text{m}$  in radius [2]. This scarring, along with localized neuronal death and gliosis, makes detecting neuronal activity very difficult and can decrease the overall performance of an electrode [3,4]. Recently, multiple groups have demonstrated minimal scar tissue around electrodes that are less than 15  $\mu\text{m}$  in diameter [5, 6, 7]. Obviously, many

This work was financially supported by the National Institute of Neurological Disorders and Stroke (1U01NS094375-01) and the McKnight Foundation.

S. P. Marshall, is with the Department of Mechanical and Biomedical Engineering, University of Michigan, Ann Arbor, MI 48109 USA ( e-mail: shamash@umich.edu).

Wei-Chen Lin, is with the Department of Mechanical Engineering, University of Michigan, Ann Arbor, MI 48109 USA and with the Advanced Institute of Manufacturing with High-Tech Innovations, Chiayi, 62102, Taiwan ( e-mail: lweichen@umich.edu).

P. R. Patel, is with the Department of Biomedical Engineering, University of Michigan, Ann Arbor, MI 48109 USA ( e-mail: parasp@umich.edu).

A. J. Shih, is with the Department of Mechanical Engineering and Biomedical Engineering, University of Michigan, Ann Arbor, MI 48109 USA ( e-mail: shih@umich.edu).

C. A. Chestek, is with the Department of Biomedical Engineering, Electrical Engineering and Computer Science, Neuroscience, & Robotics, University of Michigan, Ann Arbor, MI 48109 USA ( e-mail: cchestek@umich.edu).

electrode materials at this size scale cannot self-insert into the brain. Carbon fibers, which have a 51% higher Young's Modulus than silicon, have been shown empirically to self-insert hundreds of  $\mu\text{m}$  into cortex unassisted at a diameter of 7-8  $\mu\text{m}$  [1,5,8]. Large scale array manufacturing and animal testing can be time consuming and costly. It would better to know before beginning this process whether a particular cellular scale electrode will self-insert. However, insertion success has been difficult to quantitatively predict with a single model due to the brain having a large range of elastic moduli, specifically 0.18 – 180 kPa for the human brain [9,10] and 14.7 – 30.8 kPa for the rat brain [11]. Characterization can also be difficult when  $\mu\text{m}$  scales effects are accounted for, such as dislocation starvation which makes materials stronger at the micron scale compared to larger scale geometries [12]. Brain mimicking phantoms, typically made of agarose or gelatins, are often used for electrode insertion tests [13], but the mechanical properties of such phantoms can be difficult to match precisely to brain tissue [14] and can degrade quickly during experiments [15,16], making them hard to use for reliable predictions. In this paper, we evaluate mathematical models of beam buckling and develop a novel brain insertion phantom that can best reproduce the insertion success data of carbon electrode arrays we reported in [1].

## II. MATERIALS & METHODS

### A. Theoretical Analysis

For analyzing electrode design, material selection focused on the most commonly used electrode materials platinum, iridium, carbon fiber, and silicon with their respective compressive elastic modulus listed in [17]. It is known that the elastic modulus for each material at the micro scale is likely to be larger than reference values due to a material behavioral effect called dislocation starvation [12]. However, because only a small difference was reported, a non-microscale elastic modulus was used in our analysis.

There are three possible electrode failure conditions that could be considered during insertion tests, bending/yielding, rupture, and buckling. Rupture occurs when a compressive axial force is applied to the electrode tip and the ultimate compressive strength is reached. This is considered unlikely to happen in the case of electrodes because the ultimate compressive strength is very high that critical buckling stress is generally much lower. Rupture and yielding of the material would occur closely together in compression and we know the compressive strength is larger than the tensile strength. This is illustrated in Fig. 1 where a typical comparison is shown between the length of the electrode to the critical stress needed in order to satisfy failure stress conditions. Depending on the length of the electrode, we can see which failure condition will dominate [18, 20]. Rupture

and yield strength failures are primarily dependent on material properties with critical stresses remaining constant with electrode geometry. Buckling failure on the other hand is a common mode of failure when inserting very small electrodes. It is highly dependent on the geometry of the electrode and can be detrimental to both insertion alignment, preventing the electrode from reaching the designated target depth, and prevention of electrode penetration or fracturing of the brain tissue [19]. Therefore, we focused entirely on critical buckling strength for our model.

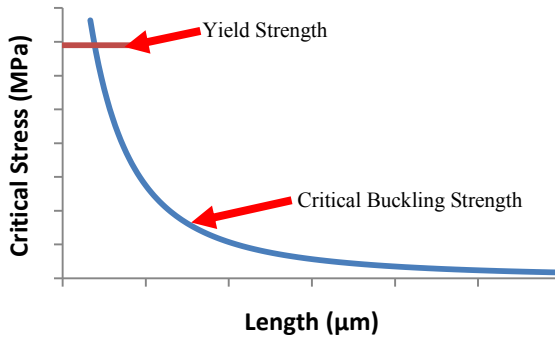


Figure 1- Critical failure stress to lengths in relation to failure conditions.

Buckling failure was defined by using Euler's Column Formula, Eq. (1), calculating the critical buckling force,  $P$ , and Eq. (2) calculating the critical buckling stress,  $\sigma$ , which the following equations are dependent on the length of the electrode,  $L$ , the elastic modulus,  $E$ , the diameter,  $D$ , and pre-determined buckling mode conditional constant,  $n$  [21]. Strengths for particular electrode geometries during insertion can also be found.

$$P = \frac{n\pi^2 EI}{L^2} \quad (1)$$

$$\sigma = \frac{n\pi^2 EI}{AL^2} \quad (2)$$

For modeling purposes, a cylindrical geometry was considered for all theoretical analyses. The relative area moment of inertia,  $I$ , and cross-sectional area,  $A$ , is described by Eqs. (3) and (4), respectively.

$$I = \frac{\pi D^2}{64} \quad (3)$$

$$A = \frac{\pi D^2}{4} \quad (4)$$

It was also possible to rearrange Eq. (1) to calculate critical buckling lengths, Eq. (5) and critical buckling diameters, Eq. (6) with a given force input.

$$L = \sqrt{\frac{n\pi^3 ED^2}{64P}} \quad (5)$$

$$D = \sqrt{\frac{64PL^2}{n\pi^3 E}} \quad (6)$$

There are five buckling modes in the mode conditional constant,  $n$  for Euler's Column Formula Eq. (1) [21]. In

order to determine which buckling mode is most important to our insertion model, we conducted several insertion experiments, described below in more detail using 5 mm length carbon fiber electrodes and compared the visually observed buckling to the modes shown in Fig. 2. Final buckling mode conditional constant selected can be seen in results.

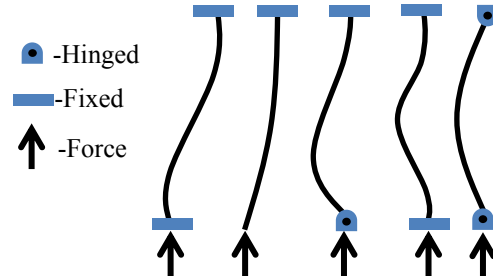


Figure 2- Showing 5 buckling modes with either fixed, hinged, or free ends.

Utilizing Euler's Column Formula, Eq. (1), as a base to our model following the selection of constant,  $n$ , critical lengths and diameters were calculated based on force values from 500 - 1000  $\mu$ N based on force probe measurements taken in [18] and compared to the requirements needed to reach a target penetration depth of 1,500  $\mu$ m. As shown by [22] and others, the most neuron rich region in a rat brain is at a depth of 1,500  $\mu$ m.

#### B. Gellan Gum Mixture

Gellan gum is an anionic polysaccharide commonly used as a substitute gelling agent in foods to replace agar, but has extended into various applications in microbiology and pharmaceuticals [8]. By adjusting the concentrations of these materials in the mixture we can create a phantom with a targeted elastic modulus,  $E$ , thermal conductivity,  $k$ , and/or electrical conductivity,  $\sigma_{Elec}$ . For our studies we focused on adjusting the mechanical properties by varying the mixture ratios. Gellan gum was used within a mixture of propylene glycol (PPG), sodium chloride (NaCl), and deionized water to create a range of phantoms with elastic modulus between 5.48 - 17.41 kPa [13] with the possibility of expanding this range depending of mixture. A regression fit model, represented by Eqs. (11), (12), and (13), was developed that can accurately calculate the necessary mass fractions of the Gellan gum,  $m_{Gellan}$ , PPG,  $m_{PPG}$ , NaCl,  $m_{NaCl}$ , and deionized water to achieve a desired elastic modulus. Variables also used in the regression model was Poisson ratio,  $v$ , and indenter radius,  $R$ , form the durometer used in measuring the elastic modulus [23].

$$E = \frac{(1-v^2)(323.852 + 8130.236m_{Gellan} + 166.169m_{PPG})}{(83.54 - 651.458m_{Gellan} - 13.290m_{PPG})^{3/2}\sqrt{R}} \quad (7)$$

$$K = 0.576 - 0.986m_{Gellan} - 0.36m_{PPG} \quad (8)$$

$$\sigma_{Elec} = 0.260 - 0.399m_{PPG} + 1.355m_{NaCl} - 2.166m_{PPG}m_{NaCl} \quad (9)$$

Utilizing this regression model, we developed a range of elastic modulus mixing ratios that fit around published elastic moduli of approximately 17 kPa to 28 kPa [11]. The mass fractions for each material found using the regression model were first weighed in a 500 g limit beaker using a

digital scale and then mixed using wooden spatula. After mixing the samples were placed in a convection oven pre-set to 220°C covering the top of the beaker with aluminum foil. Then each phantom sample was taken out of the convection oven to mix every 12 minute. After a total of 4 times mixing the samples or a total of 48 minutes in the oven, the samples were quickly taken out of the oven and poured into molds to cool for approximately 3 hours. Some alterations to equations and phantom heating in [13] were changed in order to fit our experiments.

#### D. PVC Mixture

Polyvinyl chloride (PVC) phantoms were also produced using mixture of PVC with plasticizer and various weight ratios (M-F Manufacturing 2228LP-5 plastisol and 4228S-5 plastic softener). Properties unique to PVC phantoms are that they fracture at low stresses and a wide range of mixture ratios can be obtained which directly translate into a wide range of elastic modulus possibilities. Using a 500 g capacity beaker, three mixtures ratios of 1 part plastisol to 2.2, 2.5, and 3 parts plastic softener were made. Each mixture needed to be heated to 150°C using a hot plate with a magnetic stirrer, before being placed in a vacuum chamber to remove air bubbles in the solution. The vacuum chamber was run for 1 minute at a pressure of 90 kPa before pouring the mixtures into a non-stick muffin pan or custom made rectangular Plexiglas cut out. The mixtures had to sit for 2 to 3 hours to completely settle and cool to ambient temperature. A durometer plus an automatic linear stage combination was used to determine the elastic modulus, E, of each sample made of the gellan gum and PVC phantoms. Test methods followed standard reference testing guidelines [23] and Eqs. (10), (11), and (12) with force, F, indenter radius, R, indenter height, h, indenter durometer reading, H, and poisson ratio of sample, v.

$$E = \frac{(1-v^2)F}{4h^{3/2}\sqrt{R}} \quad (10)$$

$$F = 0.01765(H) + 0.167 \quad (11)$$

$$h = 0.005 \left(1 - \frac{H}{100}\right) \quad (12)$$

#### E. Carbon Fiber Electrode Array

Electrode arrays were made using custom printed circuit boards (PCBs) with exposed traces at the tip. Carbon fibers were affixed to the exposed traces using heat cured silver epoxy [1]. Carbon fibers had a 6.8  $\mu\text{m}$  diameter and individually separated from a carbon fiber bundle (T-650/35 3K, Cytec Thornel, Woodland Park, NJ).

#### F. Insertion Experiments

Insertion experiments were conducted using a one axis manual micromanipulator with millimeter and optional micron increment motion. The micromanipulator was mounted to a threaded steel rod screwed into a larger table base. A custom designed PCB holder was 3D printed out of acrylonitrile butadiene styrene (ABS) plastic for mounting the carbon fiber array to the micromanipulator. A camera (PTEM model 12092600041) with optics (PTEM model 25479) and a variable intensity lighting system (FOSTEC LR92240) was used to capture images of buckled carbon

fibers. This setup was needed for stress analysis and provided a live feed of the insertion process. The camera's 3 axis motion and position were recorded using RSF Elektronik MSA 6506 linear encoders. The samples to be tested were placed in a custom made laser cut Plexiglas container and mounted between two solid aluminum walls to prevent external wind or lighting interferences. A white backdrop was made using standard printing paper; this allowed the camera to acquire clear images of the carbon fibers. Carbon fiber electrodes were inserted at an approximate speed of 0.4 mm/s, similar to speeds used for agarose phantom tests [15], until the PCB base came in contact with test phantom.

### III. RESULTS

#### A. Buckling Analysis

We considered the two most likely buckling modes for comparison with fiber insertion testing on gellan gum as shown in image Fig. 3. Our experimentally observed results most closely agreed to a buckling mode where one side was fixed and the other side hinged. The elasticity of the phantom did not allow for the fibers to slide across the surface thus eliminating the possibility of the other buckling mode one with one side fixed and one side free. Based on these results, a buckling mode parameter, n, of 2.045 (for the buckling mode of (2)) was chosen. This approach is based on two key assumptions: (1) the transverse load on the carbon fiber is negligible and (2) the geometry, not the end condition, is used as the criterion for selecting n.

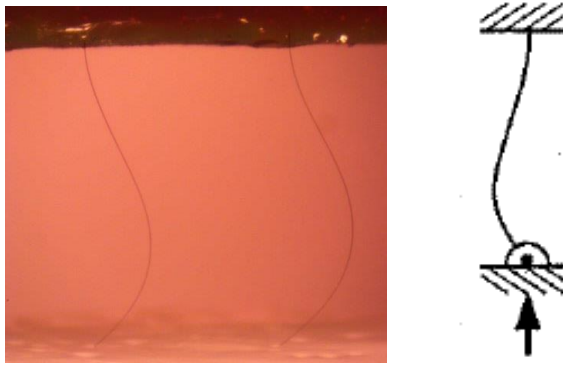


Figure 3- Observed by the buckling form of the electrodes (left) insertion attempt into Gellan Gum we can choose between the two buckling modes the electrode could fall under (right).

We then used the buckling equations to predict the insertion properties of a carbon fiber electrode with cylindrical geometry. Specifically compared critical buckling lengths to electrode diameter from a range of 5 - 10  $\mu\text{m}$  with an applied force range of 500 - 1000  $\mu\text{N}$  as shown in Fig. 4. This analysis predicts the maximum penetration depths that can be reached for specified electrode diameters that gives a basis for the size electrodes needed for insertion experiments. For a selected electrode diameter of 6.8  $\mu\text{m}$  we can compare theoretical values shown in Figs. 4 and 5 to the insertion success Fig. 6 values. From this we can see that for the range of forces between 500 - 1000  $\mu\text{N}$  there was a high insertion success rate around what is the expected

critical buckling length. The 500  $\mu$ N can be considered too small of a force for future calculations while 1000  $\mu$ N is a closer approximation to the actual force applied with a safety factor of approximately 1.25. For 90 – 100 % insertion success rate we can approximate that the critical buckling length to be 750  $\mu$ m and can further approximate the force to be 750  $\mu$ N using Fig. 4. This approximation is very similar to reference force of 780  $\mu$ N measured in [1].

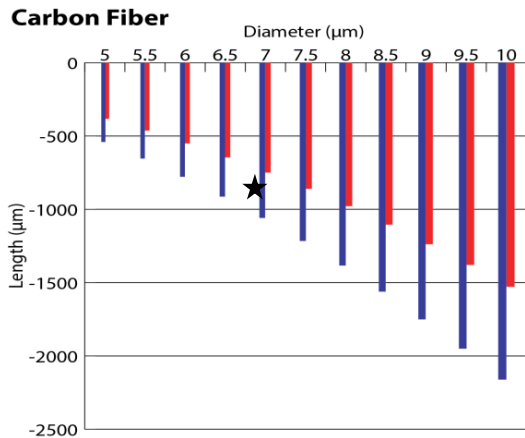


Figure 4- A linear trend can be seen for penetration depths to increasing diameters. Red lines represent penetration depths for 1000  $\mu$ N and blue lines represent for 500  $\mu$ N. The star represents approximate penetration depth and critical buckling force for 6.8  $\mu$ m diameter electrode used in our experiments.

Since the model produced results that were reasonably in alignment with our experimental results using carbon fiber, we further used that model to calculate the theoretical required diameter to reach 1,500  $\mu$ m insertion depths using a maximum force 1000  $\mu$ N applied to electrode tip. Results are shown in Fig. 5 for all materials. While the best insertion performance is predicted for Iridium and Tungsten, many common electrode materials come in below 15  $\mu$ m, suggesting that there may be a large design space for cellular scale electrodes that self-penetrate. The model also shows good agreement with experiments that the softer common materials, which better match the brain's stiffness, unfortunately will not insert at cellular diameters.

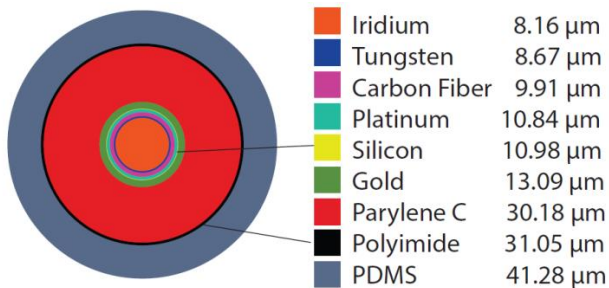


Figure 5- Diameters to reach 1,500  $\mu$ m applying 1,000  $\mu$ N.

### B. Gellan Gum Phantom Tests

The exact elastic modulus pertaining to reference values of the brain could be well matched by a gellan gum mixture developed using the regression model. However, during insertion experiments using the gellan gum phantom of the required stiffness, the carbon fiber electrodes would never

fracture the phantom and insert. Further analysis shows that although the mechanical properties can be highly customizable in terms of elastic modulus, the gellan gum mixture had too high of a fracture strength and even larger strain effects. This showed that gellan gum was not a suitable material for use in brain phantom characterization insertion tests and an alternative material had to be sought out. Thus while gellan gum has demonstrated usefulness in modeling stress at particular depths in the brain using techniques in [23,24], which is important for other aspects of electrode design, it did not work in this case for modeling insertion.

### C. PVC Phantom Tests

Carbon fiber insertion success results using PVC phantoms are shown in Fig. 6. As the plastic softener mixture ratio decreases the curves tend to converge onto the reference values [1]. An elastic modulus of 5 kPa, 7 kPa, and 8 kPa for PVC mix ratio 1:3, 1:2.5, and 1:2.2, respectively, was measured using the indenter method. These elastic modulus values are slightly outside the expected rat brain elastic modulus range of 14.70 – 30.77 kPa [11], but the data trend in Fig. 6 shows that as the amount of plastic softener decreased, there was a predictable increase in the PVC elastic modulus and continuing to decrease the amount of plastic softener will acquire a better fit insertion success curve to the referenced data. Results from real carbon thread insertion testing from [1] are shown overlaid on these curves. While agarose results are overly optimistic, the PVC mixture of 1:2.2 with 8 kPa most closely matches the brain data. These results suggest that PVC phantoms are more suitable for brain phantom characterization insertion tests than Gellam gum or agarose, can be highly customizable in term of the elastic modulus, and can mimic fracture strength to that of *in vivo* rat brains. An unexpected result from PVC phantom insertion tests was that the speed of insertion had a large impact on insertion success. At faster speeds the insertion success would increase and shift the curves in Fig. 6 to the right, while at slower speeds the insertion success would decrease and shift the curves to the left.

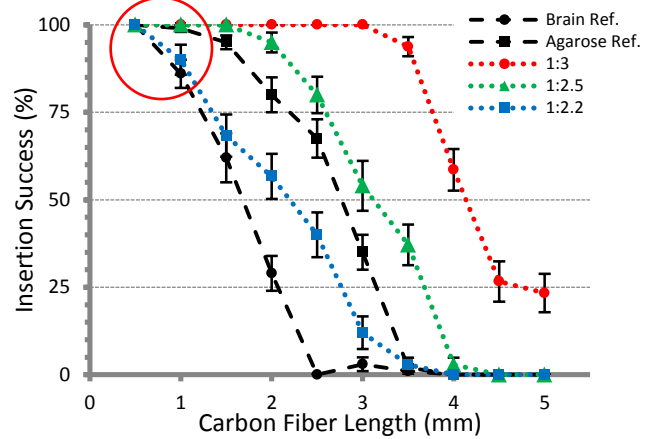


Figure 6- Relative error was associated with inserting approximately 70 fibers. Black lines are referenced data and colored lines are experiment data. Circled section is electrode insertion success between 90-100%

#### IV. DISCUSSION

In this project, we matched both a mathematical model of beam buckling, and a brain insertion phantom to our previously published data using 6.8  $\mu\text{m}$  carbon thread electrodes [1]. Overall, these results suggest two things. First, there may be an unexpectedly large design space below 15  $\mu\text{m}$  for many common electrode materials. There is only a few micron range between cellular scales and insertion failure, but this may be enough to create a range of solutions. While tungsten is well established for inserting 12  $\mu\text{m}$  micro wires into the brain, we predict that even silicon may insert without buckling at approximately 11  $\mu\text{m}$  width. Second, in terms of mechanical brain phantoms, we were best able to match our published data using PVC phantoms at mixture ratio 1:2.5 with an 7 kPa elastic modulus compared to agarose phantoms and mixture ratio 1:2.2 with an 8 kPa elastic modulus compared to brain. Gellan gum did not allow electrodes to break the surface, and agarose made overly optimistic predictions. An in depth analysis has shown the capabilities of a cylindrical carbon fiber electrode and a similar analysis can now be applied to other electrode materials and geometries. Future work will be needed for further phantom characterization, implementation and analysis of electrode support structures, validation with insertion tests for different electrode materials, and potentially in vivo rat brain insertion tests in order to provide additional parameters that can be adjusted in the model. Better characterization of the PVC brain phantoms at a larger elastic modulus would give a better understanding of the limitations of PVC. Conducting insertion tests with different electrode materials like tungsten or iridium would be needed for further validation of the electrode model. With more validation and design considerations implemented into the model we will be able to represent the entire insertion process with an array of electrodes. Strong recent chronic histological results from cellular scale electrodes [5, 25] have suggested that future designs at this size scale will substantially outperform conventional electrodes in long-term implantation. The two models presented here may aid in the development of future designs at these size scales.

#### Acknowledgment

Special thank you to the National Institute of Neurological Disorders and Stroke (1U01NS094375-01) and the McKnight Foundation.

#### REFERENCES

- [1] Patel PR, Na K, Zhang H, Kozai TDY, Kotov NA, Yoon E, Chestek CA, 2015, Insertion of linear 8.4  $\mu\text{m}$  diameter 16 channel carbon fiber electrode arrays for single unit recordings. *J. Neural Eng.* 12
- [2] Biran R., Martin D., Tresco P., 2005, Neuronal cell loss accompanies the brain tissue response to chronically implanted silicon microelectrode arrays, *Experimental Neurology*, Volume 195, Issue 1, Pgs. 115-116
- [3] Polikov V S, Tresco P A and Reichert W M 2005 Response of brain tissue to chronically implanted neural electrodes *J. Neurosci. Methods* 148 1–18
- [4] McConnell G C, Rees H D, Levey A I, Gutekunst C-A, Gross R E and Bellamkonda R V 2009 Implanted neural electrodes cause chronic, local inflammation that is correlated with local neurodegeneration *J. Neural Eng.* 6 56003
- [5] Kozai T D Y, Langhals N B, Patel P R, Deng X, Zhang H, Smith K L, Lahann J, Kotov N A and Kipke D R 2012 Ultrasmall implantable composite microelectrodes with bioactive surfaces for chronic neural interfaces *Nat. Mater.* 11 1065–73
- [6] Skousen J., Merriam M., Srivannavit O., Perlin G., Wise K., Tresco P., 2011, Reducing surface area while maintaining implant penetrating profile lowers the brain foreign body response to chronically implanted planar silicon microelectrode arrays, *Progress in Brain Research*, Volume 194, Ch. 12
- [7] Seymour J., Kipke D., 2013, Neural probe design for reduced tissue encapsulation in CNS, *Biomaterials*, Volume 28, Issue 25, Pgs. 3564-3607
- [8] Guitchounts, G., Markowitz J., Liberti W., Gardner T., 2013, A carbon-fiber electrode array for long-term neural recording, *J. Neural Eng.* Volume 10, Number 4
- [9] Clatz, Olivier, Delingette, Hervé, Talos, Ion-Florin, Golby, Alexandra J, Kikinis, Ron, Jolesz, Ferenc A, Ayache, Nicholas, & Warfield, Simon K. 2005. Robust nonrigid registration to capture brain shift from intraoperative MRI. *IEEE Trans Med Imaging*, 24(11), 1417–1427.
- [10] Kyriacou, S.K., Davatzikos, C., Zinreich, S.J., & Bryan, R.N. 1999. Nonlinear elastic registration of brain images with tumor pathology using a biomechanical model [MRI]. *IEEE Trans Med Imaging*, 18(7), 580–592.
- [11] Karimi Alireza, Navidbakhsh Mahdi, 2014, An experimental study on the mechanical properties of rat brain tissue using different stress-strain definitions, *J Mater Sci: Mater Med*, 25:1623–1630
- [12] Greer, Julia R., Nix, William D., 2006, Nanoscale gold pillars strengthened through dislocation starvation, *APS Jour. Vol.* 73 Pg. 24510-24516
- [13] Chen K Roland, Shih J Albert, 2013, Multi-modality gellan gum-based tissue-mimicking phantom with targeted mechanical, electrical, and thermal properties, *IOP Publishing: Phys. Med. Biol.* 58: 5511–5525
- [14] Hellerbach A, Schuster V, Jansen A, Sommer J (2013) MRI Phantoms – Are There Alternatives to Agar? *PLoS ONE* 8(8): e70343. doi:10.1371/journal.pone.0070343
- [15] Zhi-Jian Chen, George T. Gillies, William C. Broaddus, Sujit S. Prabhu, Helen Fillmore, Ryan M. Mitchell, Frank D. Corwin, Panos P. Fatouros, A realistic brain tissue phantom for intraparenchymal infusion studies, *Journal of Neurosurgery, August 2004 / Vol.* 101
- [16] Chen Z J, Gillies G T, Broaddus W C, Prabhu S S, Fillmore H, Mitchell R M, Corwin F D and Fatouros P P 2004 A realistic brain tissue phantom for intraparenchymal infusion studies *J. Neurosurg.* 101 314–22
- [17] Elastic Modulus Web Elements, 2015, The University of Sheffield, [webelements.com](http://webelements.com), Online College Database
- [18] Wester BA, Lee RH, and LaPlaca MC, 2009, Development and characterization of in vivo flexible electrodes compatible with large tissue displacements *J. Neural Eng.* 6
- [19] Harris JP, Hess AE, Rowan SJ, Weder C, Zorman CA, Tyler DJ, Capadona JR, 2011, In vivo deployment of mechanically adaptive nanocomposites for intracortical microelectrodes *J. Neural Eng.* 8
- [20] Najafi Khalil, Hetke Jamille, 1990, Strength Characterization of Silicon Microprobes in Neurophysiological Tissues *IEEE Transactions on Biomedical Engineering*
- [21] Akin, J., 2010, Finite Element Analysis Concepts, World Scientific, Hackensack, NJ
- [22] DeFelipe, J. (2011). The Evolution of the Brain, the Human Nature of Cortical Circuits, and Intellectual Creativity. *Frontiers in Neuroanatomy*, 5, 29. <http://doi.org/10.3389/fnana.2011.00029>
- [23] ASTM International 2010 Standard test method for rubber property—durometer hardness *ASTM Standard D2240-05* (West Conshohocken: ASTM International)
- [24] Briscoe B., Sebastian K., Adams M., 1994, The Effect of Indenter Geometry on the elastic response to indentation, *J. Physics Volume 27* Pg. 1156-1162
- [25] Xie C., Liu J., Fu T., Dai X., Zhou W., Lieber C., 2015, Three-dimensional macroporous nanoelectronic networks as minimally invasive brain probes, *Nature Materials* 14